Journal of Energy Storage 64 (2023) 107134

Contents lists available at ScienceDirect

Journal of Energy Storage

journal homepage: www.elsevier.com/locate/est

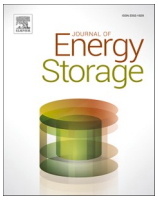

Research papers

Hydrogen diffusion into caprock: A semi-analytical solution and a hydrogen loss criterion

Mojtaba Ghaedi *, Pål Østebø Andersen, Raoof Gholami

Department of Energy Resources, University of Stavanger, Norway

ARTICLE INFO

Keywords:
Underground hydrogen storage
Diffusion
Depleted gas reservoirs
Caprock
Numerical simulation
Semi-analytical method

ABSTRACT

Depleted gas reservoirs can provide a gigaton capacity and the necessary infrastructure for large scale hydrogen storage. Therefore, underground storage of hydrogen in these geological formations is considered a valuable option. However, the high molecular diffusion of hydrogen from these storage sites is a major concern. In this paper, the idea of hydrogen diffusion through the caprock during geological storage was investigated using a series of one- and three-dimensional numerical models. In these models, the caprock and overlying formations were considered as a semi-infinite system, while the interaction between the reservoir and the caprock was defined by the pressure and gas composition at the boundary. Hydrogen diffusion was based on chemical potential differences and the influence of pre-diffused hydrocarbon gas in the caprock was considered. Furthermore, based on the analogies between the related partial differential equations of diffusion and spontaneous imbibition processes, a simple yet accurate semi-analytical solution was proposed. The presented semi-analytical solution can be used to predict the cumulative hydrogen loss over time. This solution states that the hydrogen loss increases proportionally with the square root of time. Using the semi-analytical solution, a criterion for loss by molecular hydrogen diffusion was presented that indicates the fraction of hydrogen lost by diffusion at a given time. The results obtained based on the diffusion fluxes showed that the hydrogen loss can be underestimated if the existence of hydrocarbon gas in the caprock is ignored. The analysis also indicated that hydrogen loss is directly proportional to the interface between rock and reservoir exposed to hydrogen, the caprock porosity, the gas saturation of the caprock, the square root of the diffusion coefficient, and the square root of time. While the presence of hydrocarbon gas facilitates diffusion, the thermodynamic effects at high pressures lead to a comparatively lower molar density in the caprock than in the matrix. Thus, a lower final loss of the injected hydrogen can be expected at higher pressures.

1. Introduction

Climate change and global warming due to the continuous release of greenhouse gases into the atmosphere need to be mitigated. Therefore, decarbonization of heavy industries, transportation, and aviation systems will be a crucial step toward a carbon-neutral society [1,2]. Hydrogen (H_2) has a high energy density and can undergo emission-free combustion. Thus, it can play a key role in a future carbon-free economy [3]. However, H_2 has a very low volumetric density. Thus, cost-effective large scale storage sites, such as underground geological formations, may be required to maintain smart grid stability and to balance fluctuations in energy demand [4–6].

Geological storage of H_2 can be done in salt caverns [7,8], saline aquifers [9,10], and depleted gas reservoirs [11,12]. Salt caverns are perhaps the best sites for H_2 storage. There is a long history of good experience of storing natural and town gas (with H_2 content close to 50 %) in such caverns across Europe, particularly in the UK [13,14]. However, they have a lower storage capacity than saline aquifers or depleted gas reservoirs. Furthermore, these formations are subject to cyclic injection/withdrawal fatigue and may not be available in certain geological settings or at depths that make their application practical [15,16]. Saline aquifers offer tremendous capacity for H_2 storage, but they require a large amount of cushion gas to operate [17,18]. In addition, extensive characterization is required before they can be considered as a viable storage option [19]. Depleted gas reservoirs, on the other hand, have residual gas that can serve as a buffer. Furthermore, their geological structure is known, the integrity of their caprock is proven, and infrastructure installed on the surface and underground can

* Corresponding author.
E-mail address: mojtaba.ghaedi@uis.no (M. Ghaedi).

https://doi.org/10.1016/j.est.2023.107134
Received 3 January 2023; Received in revised form 3 March 2023; Accepted 10 March 2023
Available online 23 March 2023

reduce the cost of H_2 storage [20,21]. However, impurities in the produced H_2 and possible biochemical/geochemical reactions are among the major concerns when it comes to H_2 storage in depleted gas reservoirs [22]. Visser [23] conducted a feasibility study for H_2 storage in depleted gas reservoirs and reported on the potential challenges of storage in such formations. One of these major challenges is perhaps the leakage and loss from the caprock [23].

Caprock integrity in a storage site is often assessed by capillary sealing efficiency. This efficiency depends on wettability, interfacial tension, threshold pore radius of the caprock, and fluid densities. When analyzing the capillary sealing efficiency, the impacts of temperature, pressure, salinity, mineralogy, and total organic content of the caprock should be analyzed [24,25].

Very fine-grain clays such as kaolin, smectite, and illite are the primary component of the caprock [26]. Mineralogical composition of caprock and its alteration due to the geochemical interactions with H_2/brine is another important parameter under these circumstances [27–29]. For instance, Bo et al. [30] and Gholami [31] performed a series of geochemical modeling to study H_2 loss as a function of temperature and pressure [30,31]. They reported H_2 loss due to the presence of calcite and clay minerals in a reservoir or caprock. Furthermore, the dissolution of the pyrite at high temperatures during H_2 storage is another issue raised [32].

H_2 molecular diffusion is another important but less studied mechanism when it comes to caprock quality assessment. Injected H_2 has a much lower density than the residual gas in the reservoir and forms a chamber directly under the caprock. Thus, due to its small molecular size [33] and mobility, there is a high probability of diffusion and loss from the caprock [34,35]. Fig. 1 schematically shows an underground H_2 storage (UHS) site and the potential diffusion through the caprock. As can be seen in this figure, H_2 injected into a depleted gas reservoir accumulates at the top of the reservoir directly beneath the caprock, where it has the potential to diffuse into the caprock and upper formations.

To date, several experimental and molecular dynamics simulation approaches have been used to study H_2 diffusion. For instance, Gupta et al. [36] reported a value of 3×10^{-11} m^2/s for the H_2 diffusion coefficient in water saturated clays at 25 °C [36]. A range of 6×10^{-8}–12.2×10^{-8} m^2/s was also calculated for the self-diffusion coefficient of H_2. The experiments were performed on montmorillonite clays with pore sizes of 8–40 nm and in temperature and pressure ranges of 60–140 °C and 20–300 bar, respectively [35]. Bhimineni et al. [37] used molecular dynamics simulations to estimate H_2 diffusion into brine with different cations (Na^+, K^+, Ca^{2+}) and up to a concentration of 5 mol/kgH_2O [37]. They validated the obtained simulation results in a range of 0.46×10^{-8}-1.31×10^{-8} m^2/s and 10–60 °C temperature with experimental data. Similarly, Ghasemi et al.[38] used molecular dynamics simulations to mimic H_2 diffusion through water-saturated clays and determined a range of 3.4×10^{-9}–12×10^{-9} m^2/s [38]. They considered different clay minerals such as pyrophyllite, Na-montmorillonite, Ca-montmorillonite, Na-beidellite, and Ca-beidellite with pore sizes ranging from 1 to 8 nm. In another study, the H_2 diffusion coefficient was determined experimentally in an Australian anthracite coal sample with a range of 0.99×10^{-8}–5.92×10^{-8} m^2/s [34]. The experiments were conducted at a temperature range of 20–60 °C and approximately a constant pressure of 13 bar.

This paper provides insights into H_2 diffusion through caprock during geological storage by describing the main characteristics of diffusion and analyzing the effective parameters. A semi-infinite system was considered to represent H_2 diffusion into the caprock and upper reservoir formations. The chemical potential was utilized as the driving mechanism, and the presence of previously diffused hydrocarbon gas in the caprock was considered. Based on similarities between the partial differential equation describing H_2 diffusion and spontaneous imbibition, a semi-analytical solution was proposed. The presented semi-analytical solution can be used to predict H_2 loss during the semi-infinite period. Furthermore, a loss fraction criterion was presented to quantify the severity of diffusive H_2 loss.

The paper is structured as follows: The concept of H_2 diffusion is presented, followed by general equations and system description. A semi-analytical solution is derived using the corresponding partial differential equation and the chemical potential gradient as the diffusion mechanism. The numerical simulation approach and its comparison with the analytical solution are then presented followed by sensitivity analyses of the influencing parameters. A comparison of the semi-analytical solution with the numerical simulation for several cases are presented. Finally, H_2 diffusion through the caprock is investigated using three-dimensional models. Fig. 2 shows the flowchart of this study.

2. H_2 diffusion

Molecular diffusion is defined as the mass transfer of components in a system due to the random motions of molecules [39]. Different mechanisms can be used to describe molecular diffusion including concentration gradient, temperature difference, chemical potential, and magnetic or electric fields [40]. However, when magnetic and electric fields are not present and temperature changes during H_2 injection are neglected, concentration gradients and chemical potentials are the mechanisms behind molecular diffusion. The diffusion flux based on the concentration gradient is given by [41]:

$$J_i = -CD_i \frac{\partial y_i}{\partial Z} \tag{1}$$

where J_i is the molar flux of component i, C is the total molar concentration (the inverse molar volume of the mixture), D_i is the effective diffusion coefficient of component i, y_i is the molar fraction of component i, and $\frac{\partial y_i}{\partial Z}$ is the gradient of the molar fraction of component i in the Z direction.

Although Eq. (1) is often used in diffusion modeling, it is possible for

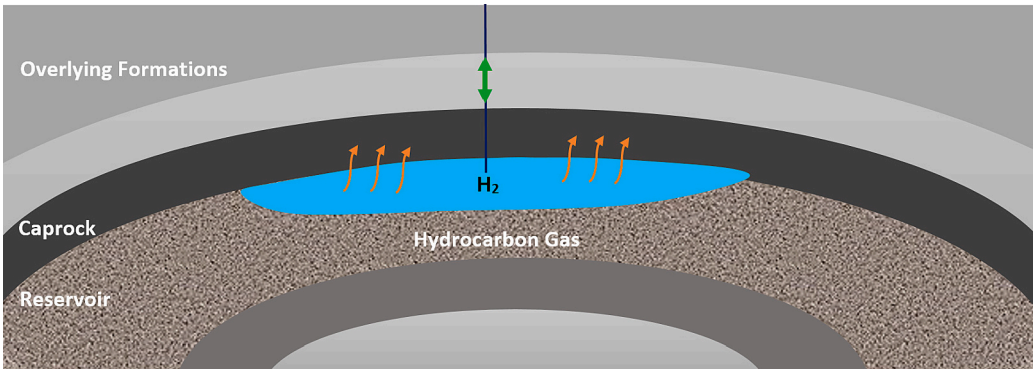

Fig. 1. H_2 storage in a depleted gas reservoir and its diffusion into the caprock.

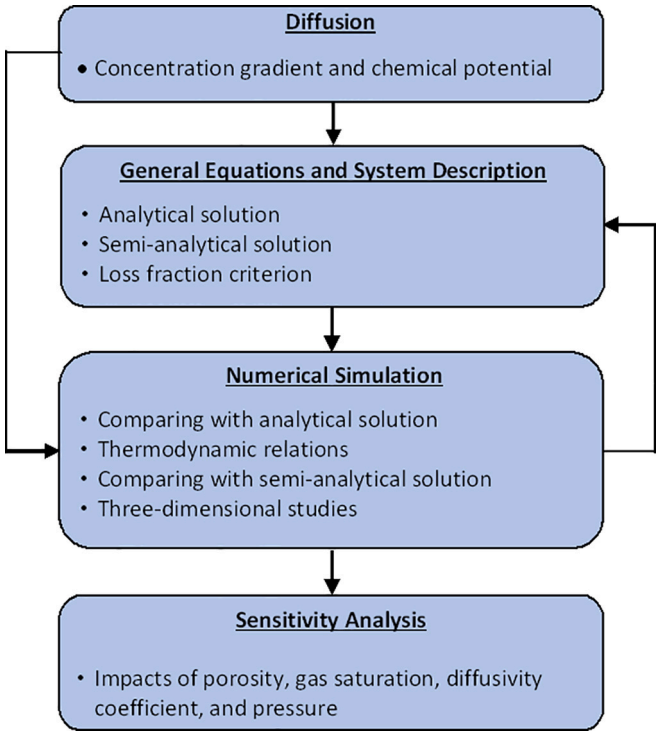

Fig. 2. The flowchart of this study.

a component to diffuse from a lower to a higher concentration. Thus, to describe the diffusion process for more general conditions, something more than just the concentration gradient should be used. For example, one can use complex composition-dependent mechanisms through intermolecular interactions under these circumstances.

The modern theory assumes that molecular diffusion is driven by the chemical potential gradient of a species [41]. H_2 diffusion in a multi-component hydrocarbon-water mixture at elevated reservoir pressure can be regarded as a non-ideal multicomponent system. Thus, to accurately describe the diffusion process, the following flux-based chemical potential gradient is applied [42]:

$$J_i = -CD_i^a y_i \frac{1}{RT}\frac{\partial \mu_i}{\partial Z} \tag{2}$$

where D_i^a is the activity-corrected diffusion coefficient of component i, T is the temperature, R is the universal gas constant, and μ_i is the chemical potential of component i. Here, μ_i is a function of the fugacity of component i (f_i) and can be addressed by [42]:

$$\mu_i = \mu_{i0} + RTln(f_i) \tag{3}$$

μ_{i0} is the reference chemical potential and the fugacity of a real gas is defined as an effective partial pressure. The flux is zero if the chemical potential is uniform.

3. General equations and system description

In a gas reservoir, the gas has been in contact with the caprock over geological time. Thus, it has been able to diffuse into the caprock [43–45]. The presence of hydrocarbon gas in the caprock must therefore be considered. Here, the flux of a component i through the area accessible to the flow (i.e., the area occupied by gas) is given by J_i ($\frac{mol}{s\ m^2}$). As a result, if Eq. (2) is combined with Eq. (3), J_i can be expressed by Eq. (4) using the fugacity or mol fraction gradient:

$$J_i = -CD_i^a y_i \frac{\partial (lnf_i)}{\partial Z} = -CD_i^a y_i \frac{\partial (lnf_i)}{\partial (lny_i)}\frac{1}{y_i}\frac{\partial y_i}{\partial Z} = -CD_i^a \frac{\partial (lnf_i)}{\partial (lny_i)}\frac{\partial y_i}{\partial Z} \tag{4}$$

Because of the low molecular density and size, H_2 will seep from the top of the reservoir into the caprock soon after injection. The interface between reservoir and caprock can be defined to be at $Z = 0$. A total reservoir molar concentration $C_0 = C(Z = 0^-, t)$ and a composition $y_{i0} = y_i(Z = 0^-)$ are then considered at $Z = 0$, and assumed to be constant (see Fig. 3). The initial composition of the caprock ($C_{i,ini}$) is known with the H_2 concentration being zero and the hydrocarbon concentration being non-zero. The system is assumed to be semi-infinite (i.e., the initial concentration is obtained as Z goes to infinity). The above conditions can be summarized as follows and explained schematically in Fig. 3:

$$C_i = C_{i,ini},\ Z > 0,\ t = 0\ [\text{Initial Condition in the Caprock}] \tag{5}$$

$$C_i = C_{i0},\ Z = 0^-,\ t > 0\ [\text{Caprock} - \text{Reservoir Interface}] \tag{6}$$

$$C_i = 0,\ Z = \infty,\ t > 0\ [\text{Far from Caprock} - \text{Reservoir Interface}] \tag{7}$$

where C_{i0} is the H_2 concentration below the caprock in the reservoir.

The flux at the caprock boundary is $J_{i0} = J_i(Z = 0^+, t)$, see Fig. 3. Diffusive transport is only considered in the gas phase, so the molar loss (and mass loss) per time into the caprock is expressed by:

$$\frac{dn}{dt} = A\phi S_g J_{i0}, \frac{dm}{dt} = M\frac{dn}{dt} \tag{8}$$

where A is the area between the caprock and the reservoir exposed to H_2, M is the molecular weight, $\frac{dn}{dt}$ and $\frac{dm}{dt}$ are molar and mass loss per time, respectively. Here, the porosity ϕ and gas saturation S_g within the caprock are assumed to be equal, resulting in a uniform flux across the surface between the reservoir and the caprock.

It seems that the continuity of chemical potential does not necessarily correspond to the continuity of species concentration. Thus, the composition C_{i0} in the reservoir can lead to a boundary concentration, C_{i^*}, which may differ from C_{i0} as addressed below:

$$C_i = C_{i^*},\ Z = 0^+,\ t > 0\ [\text{Caprock} - \text{Reservoir Interface}] \tag{9}$$

In the following section, we investigate these sets of equations theoretically to obtain a more general understanding of diffusion mechanisms. We also demonstrate how diffusion models with the boundary condition given in Eq. (9) in the caprock can provide a good estimate once compared with numerical simulations built based on Eq. (6) in the reservoir.

3.1. Semi-analytical solution

To develop a semi-analytical solution for H_2 diffusion to the caprock, first assume that the total concentration C is constant. The component concentration ($C_i = Cy_i$) can then be applied to rewrite Eq. (4) as:

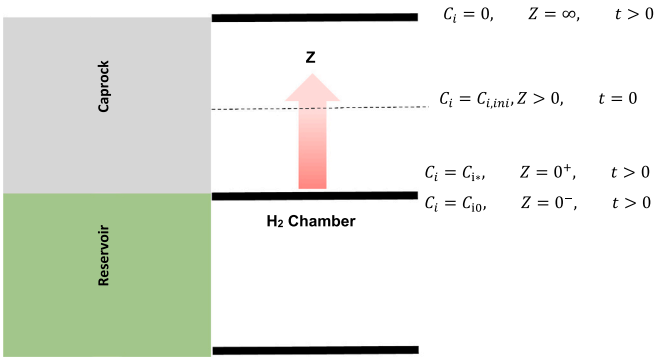

Fig. 3. H_2 diffusion through the caprock with a plane source in a semi-infinite medium.

$$J_i = -D_i^a \frac{\partial(lnf_i)}{\partial(lny_i)} \frac{\partial C_i}{\partial Z} \tag{10}$$

J_i can then be expressed using the more common form of Fick's first law (Eq. (11)) where a compact diffusion coefficient (D_i) is the only parameter to consider other than the concentration gradient:

$$J_i = -D_i \frac{\partial C_i}{\partial Z}, where\ D_i = D_i^a \frac{\partial(lnf_i)}{\partial(lny_i)} \tag{11}$$

In the above equation, D_i^a only depends on the pores and fluids configuration in the porous medium. An important point of investigation is then how the term $\frac{\partial(lnf_i)}{\partial(lny_i)}$ affects the H_2 loss through the caprock. The term $\frac{\partial(lnf_i)}{\partial(lny_i)}$ only depends on the thermodynamic of the system and in a condition where both temperature and pressure are constant, it varies only with gas composition. Thus, its dependency can be expressed by C_i and at low pressures $\frac{\partial(lnf_i)}{\partial(lny_i)} \rightarrow 1$. Then, the flux of chemical and potential driven diffusion become equal [41,42].

When performing a mass balance over an infinitesimal volume with Fick's first law (Eq. (10)) as flux, Fick's second law is obtained as [39]:

$$\frac{\partial C_i}{\partial t} = \frac{\partial}{\partial Z}\left(D_i \frac{\partial C_i}{\partial Z}\right) \tag{12}$$

In the above equation, D_i is generally not constant (due to thermodynamics) but a function of C_i. This system of equation (Eq. (12)) is mathematically similar to the description of spontaneous imbibition (in a semi-infinite system) and has a similar semi-analytical solution in integral form [46]. This semi-analytical solution states that the position of a given concentration ($Z(C_i)$) is proportional to the square root of time ($t^{0.5}$), a constant A_0 and the concentration derivative of a function $F(C_i)$ depending on concentration:

$$Z(C_i) = 2A_0 F'(C_i) t^{0.5} \tag{13}$$

In addition, J_{i0} is inversely proportional to the square root of time [46]:

$$J_{i0} = A_0 t^{-0.5} \tag{14}$$

We refer to McWhorter and Sunada [46] and Andersen [47,48] for the derivation of A_0 and $F(C_i)$ for similar systems [46–48]. The loss of H_2 at a given time is equivalent to the number of moles in the caprock (n_i). That can be expressed per gas phase volume by integrating the concentration profile along the caprock or equivalently by integrating the flux at the boundary over time:

$$\frac{n_i}{A\phi S_g} = \int_0^{C_{i^*}} Z(C_i) dC_i = \int_0^t J_{i0} dt = 2A_0 t^{0.5} \tag{15}$$

The constant factor A_0 can be evaluated accurately based on the value A_{0cD}. One can obtain the value of A_0 when the diffusion coefficient D_i is constant and is equal to its mean and by considering how much D_i is skewed to either side as a function of its input variable [47,48]:

$$\frac{n_i}{A\phi S_g} = 2\left(\frac{A_0}{A_{0cD}}\right) A_{0cD} t^{0.5} \tag{16}$$

If D_i is not highly asymmetrical, $\frac{A_0}{A_{0cD}} \approx 1$. In the next section, the value of A_{0cD} is determined analytically by considering a constant diffusion coefficient.

3.2. Analytical solution and determination of A_{0cD}

It should be recalled that when D_i is constant, Eq. (12) can be solved as [39]:

$$C_i(Z,t) = C_{i^*}\left(erfc\left(\frac{Z}{2\sqrt{D_i t}}\right)\right) \tag{17}$$

Inverting this equation, the position can be obtained as a function of concentration:

$$Z(C_i) = 2erfc^{-1}\left(\frac{C_i}{C_{i^*}}\right)\sqrt{D_i t} \tag{18}$$

The loss with time is then simply written as:

$$\frac{n_i}{A\phi S_g} = \int_0^{C_{i^*}} Z(C_i) dC_i = 2C_{i^*}\sqrt{D_i t}\int_{Y=0}^{1} erfc^{-1}(Y) dY \tag{19}$$

where $Y = C_i/C_{i^*}$. Comparing with Eq. (15), and setting $A_0 = A_{0cD}$ as D_i is constant, A_{0cD} can be calculated as:

$$A_{0cD} = C_{i^*}\sqrt{D_i}\int_{Y=0}^{1} erfc^{-1}(Y) dY = 0.5642 C_{i^*}\sqrt{D_i} \tag{20}$$

where we have used that $\int_{Y=0}^{1} erfc^{-1}(Y) dY = 0.5642$ (calculated with MATLAB using 1000 points) [49].

3.3. Hydrogen loss and a criterion for significant loss fraction

Having evaluated A_{0cD} from Eq. (20), the total loss of H_2 can be expressed using Eq. (16) as:

$$n_i = 1.128\left(\frac{A_0}{A_{0cD}}\right) A\phi S_g C_{i^*}\sqrt{D_i}\sqrt{t}, \tag{21}$$

The factor $\frac{A_0}{A_{0cD}}$ is a simple function of diffusion coefficient skewedness, with a magnitude close to 1 [47]. If the coefficient is shifted to higher concentrations, the ratio becomes higher than 1. It is less than 1 if the coefficient is shifted to low concentrations. Here, $\overline{D}_i$ is the mean of $D_i^a \frac{\partial(lnf_i)}{\partial(lny_i)}$ as addressed by Eq. (22) where only $\frac{\partial(lnf_i)}{\partial(lny_i)}$ is non-constant and responsible for adjusting the shape and magnitude of D_i:

$$\overline{D}_i = D_i^a \overline{\frac{\partial(lnf_i)}{\partial(lny_i)}}, where\ \overline{\frac{\partial(lnf_i)}{\partial(lny_i)}} = \frac{1}{C_{i^*}}\int_{C_i=0}^{C_{i^*}} \frac{\partial(lnf_i)}{\partial(lny_i)} dC_i \tag{22}$$

Assuming a reservoir with a matrix porosity of ϕ_m, a vertical H_2 column height of H, a gas saturation of S_{gm}, and an H_2 concentration of C_{i0} (assumed to be uniform in the reservoir and contacting the reservoir-caprock boundary), the amount of moles stored in the reservoir (n_m) are:

$$n_m = AH\phi_m S_{gm} C_{i0} \tag{23}$$

Assuming diffusion has occurred over a time t, the loss fraction (LF) of the stored H_2 can be calculated as:

$$LF = \frac{n_i}{n_m} = 1.128\left(\frac{A_0}{A_{0cD}}\right)\frac{\phi S_g C_{i^*}}{\phi_m S_{gm} C_{i0}}\frac{\sqrt{D_i}\sqrt{t}}{H} \tag{24}$$

In the above equation, if LF is significantly less than one, the diffusion losses in the caprock can be ignored. This can serve as a criterion for whether the reservoir will be an effective storage space or not. However, this criterion is only valid for the evaluation of diffusion. Other loss mechanisms need to be evaluated separately. In an ideal gas state $\frac{\partial(lnf_i)}{\partial(lny_i)} \rightarrow 1$, such that $\overline{D}_i \rightarrow D_i^a$, $C_{i^*} \rightarrow C_{i0}$ and $\frac{A_0}{A_{0cD}} \rightarrow 1$. The LF can then be simplified to:

$$LF_{ideal} = 1.128\frac{\phi S_g}{\phi_m S_{gm}}\frac{\sqrt{D_i^a}\sqrt{t}}{H} \tag{25}$$

To simultaneously estimate the impact of diffusion coefficient shape and magnitude (and not separately), we assumed that Eq. (19) holds also for a non-constant D_i. That leads to the following approximation of the terms in Eqs. (21) and (24):

$$1.128\left(\frac{A_0}{A_{0cD}}\right)\sqrt{\overline{D}_i} \approx 2\sqrt{D_i^a}\int_{Y=0}^{1}\sqrt{\frac{\partial(lnf_i)}{\partial(lny_i)}} erfc^{-1}(Y) dY \tag{26}$$

4. Numerical simulation

As mentioned earlier, the chemical potential gradient is the mechanism that can better explain the H_2 diffusion through the caprock. Thus, this mechanism was used to simulate the diffusion of injected H_2 from the depleted gas reservoir into the caprock. Schlumberger's commercial simulator Eclipse 300 was used together with a fully implicit compositional simulation to mimic an UHS site [42]. The Peng-Robinson equation of state was used to model the fluid properties [50] which has also been used by others to model fluid properties in an UHS [18,51,52].

As mentioned earlier, the presence of previously diffused hydrocarbon gas in the caprock was considered in this work. Therefore, it was assumed that the caprock has a two-phase system of liquid and gas in its pore structure. However, the amount of water and gas in the gas and water phases depends on the PVT conditions of the caprock. Here, 1-D models were initialized at the desired temperature and pressure, with H_2 in the reservoir and with hydrocarbon gas (such as methane) and water in the caprock in certain total mole fractions. A block with a length of 20 ft in the X and Y directions was considered and a fine grid with a size of 0.1 ft in the Z direction was used. To obtain a semi-infinite condition for the diffusion of H_2 into the caprock, the length of the caprock was fixed at 1000 ft and the molar density of H_2 in the gas phase of the caprock was determined. In addition, the H_2 concentration in the reservoir and below the interface between the caprock and the reservoir was kept constant to obtain a constant concentration boundary. In addition, the liquid and gas phases were immobile due to the impermeability of the caprock, so both phases were assigned a relative permeability of zero. It should be noted that the focus of this work is on the assessment of H_2 loss by diffusion into the caprock and possible chemical and biochemical reactions were not considered. Fig. 4 shows an example of a 1-D model created for this study to simulate the diffusion with the reservoir initially filled with H_2. As this figure shows, the H_2 concentration in the reservoir is constant and it diffuses into the caprock over time.

Fig. 5 gives an example of the H_2 fugacity trends at the top of the reservoir and at a distance of 5 ft. above the caprock-reservoir interface together with the H_2 concentration profiles. This simulation was performed at 3000 psi pressure and 173 °F. The differences between the fugacity in the caprock and reservoir result in molecular diffusion. The H_2 concentration in the caprock remains constant once the fugacity of the caprock and the reservoir are equal. As can be seen, the final H_2 concentration in the caprock (C_{i^*}) is less than the H_2 concentration below the interface between the caprock and reservoir (C_{i0}).

4.1. Comparing numerical and analytical solutions

To assess whether the 1-D simulation model and the analytical solution presented earlier (*erfc* solution) are in good agreement, a series of analyses were done. In all models, a range of 10^{-7} to 10^{-10} m^2/s was considered for D_i^a in the numerical simulation and for D_i in the analytical solution with a porosity of 10 % for the caprock. The results obtained are shown in Fig. 6. The comparisons between the concentration profiles

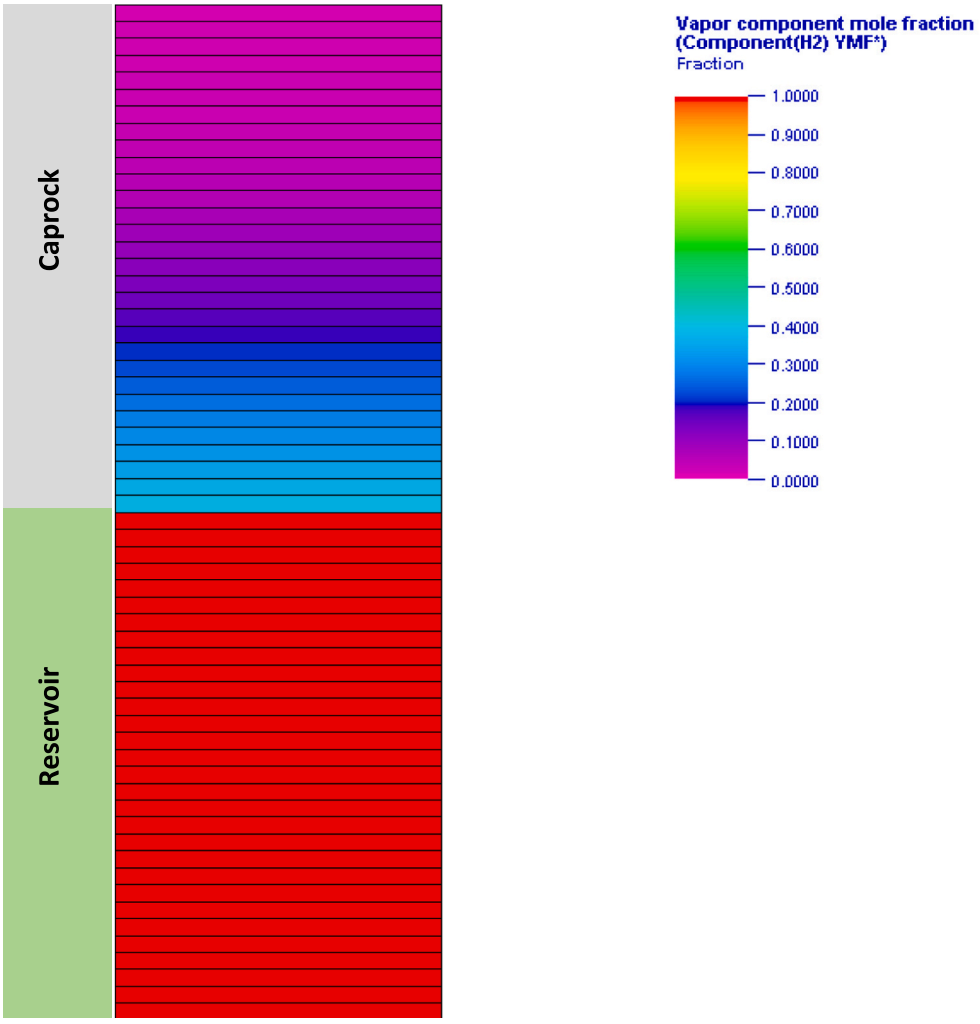

Fig. 4. Example of H2 mole fraction in the gas phase due to diffusion from the reservoir to the caprock.

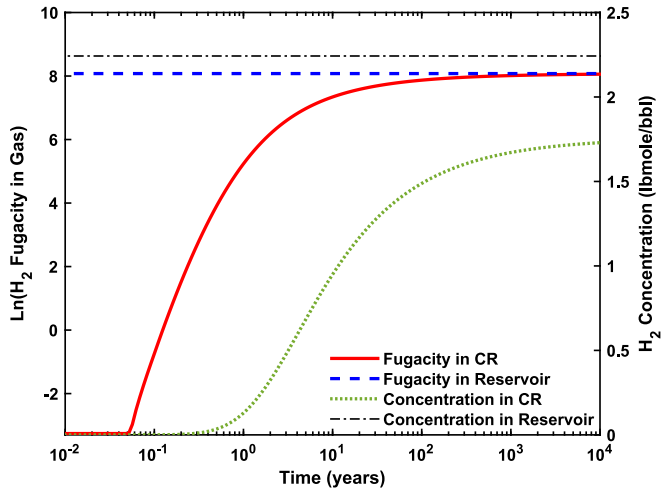

Fig. 5. H_2 fugacity and concentration profiles at 5 ft. above the caprock-reservoir interface and at the top of the reservoir.

were plotted against time at a distance of 5 ft. above the caprock (Fig. 6. a) and after 10 years along the caprock (Fig. 6.b). It should also be mentioned that the simulation was performed at a low pressure of 200 psi (84 °F) to have similar chemical potential and concentration driven diffusion fluxes. Also, methane (C_1) was considered in the caprock. As can be seen in Fig. 6, good agreement is observed between the analytical and numerical solutions at low pressure with respect to the profile shape.

Fig. 7 shows another comparison between numerical and analytical solutions at a high pressure of 4000 psi and a temperature of 205 °F. This figure shows the H_2 concentration at a distance of 5 ft. above the caprock-reservoir interface where D_i^a was 10^{-8} m^2/s. A similar value was considered for D_i in the analytical solution and the porosity of the caprock was 10 %. The H_2 boundary concentration directly below the caprock in the reservoir (C_{i0}) was used for the analytical solution. A look at Fig. 7 shows that the analytical solution has a rapid and higher diffusion soon after H_2 injection. Fig. 7 further highlights the difference between the final H_2 concentration in the caprock (C_{i^*}) and the H_2 boundary concentration just below the caprock in the reservoir (C_{i0}). It should be noted that the area covered by H_2 and the local composition and pressure of H_2 along the caprock vary with time while the analytical solution is based on constant values. Thus, certain differences in the concentration profiles obtained from the numerical and analytical solutions are to be expected. The H_2 concentration in the analytical solution eventually reaches C_{i0} (2.75 lbmole/bbl) while the numerical solution approaches lower concentrations in the caprock (1.95 lbmole/bbl). Thus, it can be concluded that the chemical potential can better represent H_2 diffusion through the caprock at elevated pressure, as already pointed out by [53].

4.2. Thermodynamical relations

In this section, we investigate the relationship between boundary concentrations C_{i^*} and C_{i0} at different reservoir pressures and temperatures. We also evaluate the term $\frac{\partial(lnf_i)}{\partial(lny_i)}$ against $\frac{C_i}{C_{i^*}}$ at different pressures. These relationships can be used in the semi-analytical solution or in the criterion to evaluate the loss fraction.

Fig. 8 gives the relationship between C_{i^*} and C_{i0} calculated using the Peng-Robinson equation of state [50] in the presence of C_1 in the caprock and H_2 in the reservoir. Normal temperature and pressure gradients of 15 °F/1000 ft. and 0.465 psi/ft., respectively, were considered to calculate H_2 concentrations in the reservoir and caprock. In this figure, pressures ranged from 200 to 4000 psi and temperatures accordingly ranged from 84 to 205 °F. At higher pressure, the molar density of H_2 increases in both the matrix and the caprock, but the equality of chemical potential and the presence of C_1 results in a lower molar density in the matrix at higher pressure. This highlights the fact that the thermodynamic interaction between C_1 and H_2 limits the H_2 diffusion loss.

Based on Eq. (10), D_i and D_i^a are related by the term $\frac{\partial(lnf_i)}{\partial(lny_i)}$. Fig. 9 shows $\frac{\partial(lnf_i)}{\partial(lny_i)}$ vs. $\frac{C_i}{C_{i^*}}$ at pressures of 200, 1500, and 3000 psi. At higher pressures and concentrations, the term $\frac{\partial(lnf_i)}{\partial(lny_i)}$ becomes higher than 1. Both the increase in magnitude and the shift to high concentrations, increase the diffusion rate toward the maximum concentration [47,48]. As shown in Fig. 8, this maximum concentration C_{i^*} also increases with pressure, but to a lesser extent than the concentration in the reservoir C_{i0}. This will be investigated further with dynamic simulations. At low pressure (200 psi) the function of $\frac{\partial(lnf_i)}{\partial(lny_i)}$ versus $\frac{C_i}{C_{i^*}}$ is approximately constant and equal to 1. This shows that at a low pressure the effects of the chemical potential are negligible.

4.3. Sensitivity analysis

In this section, H_2 diffusion into the caprock is evaluated using the 1-D numerical models. In particular, the effects of different parameters such as gas saturation and caprock porosity, diffusion coefficient, and reservoir pressure are evaluated. For all cases, the following three parameters are used to evaluate H_2 diffusion:

- Loss of moles over 30 years ($n_{i,30}$)
- Flux (per total area) at the caprock interface averaged over 30 years ($\overline{(J_{i,30}\phi S_g)}$ where $\overline{J_{i,30}}\phi S_g = n_{i,30}/(30A)$ (Eq. (15))
- The coefficient $A_0\phi S_g$ related to flux per total area ($J_{i0}\phi S_g = (A_0\phi S_g)t^{-0.5}$ (Eq. (14)).

The period of 30 years was selected as an estimate for the short-term economic lifetime of H_2 storage operations [54].

4.3.1. Caprock gas saturation and porosity

To better understand the role of S_g on H_2 diffusion, models were created with different S_g. In these models, the total mole fractions of C_1 (Z_{C1}) were changed from 0.01 to 1, resulting in gas saturation ranging from 5.5 to 100 %. In these models, the pressure is 3000 psi, D_i^a is 10^{-8} m^2/s, and the caprock porosity is 10 %. Fig. 10.a shows the H_2 concentration in the gas phase at a distance of 5 ft. above the caprock-reservoir interface. It should be noted that multiplying the H_2 concentration by the corresponding S_g gives the concentration per pore volume. Fig. 10.b shows the cumulative H_2 loss per unit area (n_i/A) versus the square root of time over 100 years for different gas saturations. As this figure suggests the trend of n_i/A against the square root of time is linear. The parameters of the H_2 concentration profiles including $n_{i,30}$, $\overline{J_{i,30}}\phi S_g$, and $A_0\phi S_g$ are given in Table 1. All these parameters are proportional to the relevant S_g at different Z_{C1}.

Based on Table 1, the differences between H_2 loss at different Z_{C1} in the caprock are considerable. Several studies have shown that water saturation of the caprock decreases due to gas diffusion [55–57]. This suggests that more space is available for H_2 in the gas phase when the diffusion of hydrocarbon gas into the caprock is considered. Thus, one might underestimate H_2 loss by diffusion if the pre-existence of hydrocarbon gas in the caprock is neglected. Further investigations are required for more accurate determination of thermodynamic conditions of gas and water in the caprock as this issue depends on various conditions, including gas adsorption, caprock fractures, water salinity, and heterogeneities [55,58].

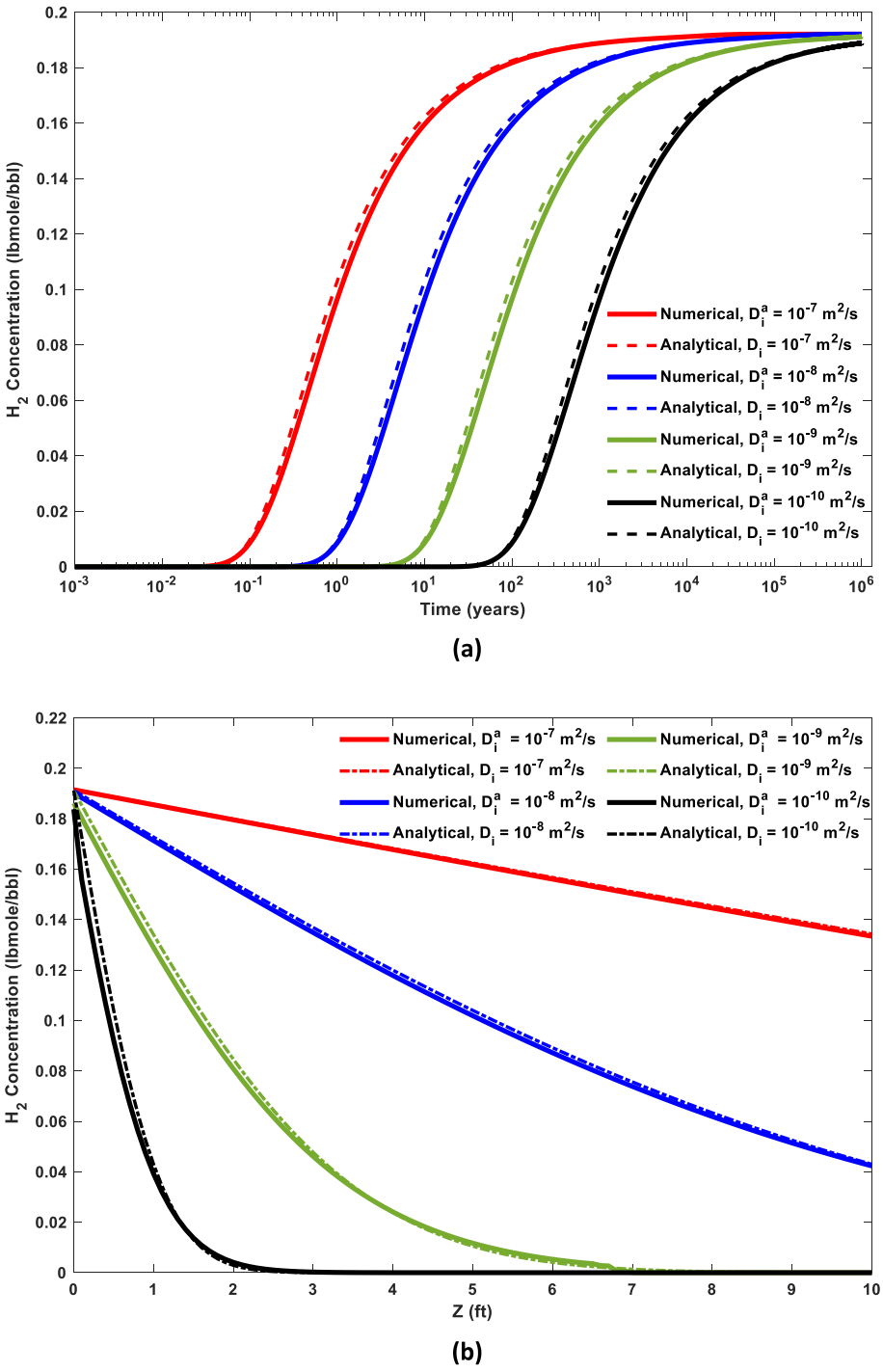

Fig. 6. Comparison of the analytical and numerical solutions for H_2 diffusion profiles through the caprock, (a) at 5 ft. above the caprock vs. time, (b) after 10 years along the caprock.

Caprocks such as shale are considered to have low effective porosity and incredibly low permeability [59]. Porosity represents the amount of pore volume available in the caprock. It is thus a factor that influences the amount of H_2 diffusion. For this reason, different models with different ϕ values from 1 to 10 % were created. In these models, the pressure and Z_{C1} were 3000 psi and 5 % respectively. It should be noted that the D_i^a depends on the pore structure of the caprock. Therefore, the values of D_i^a may vary depending on the porosity. However, in this work, a constant D_i^a value was considered for different models with different porosities to study the effects of porosity on H_2 diffusion. Fig. 11 and Table 2 show the effects of ϕ on the H_2 concentration in the caprock. Similar to gas saturation, the same evolution of H_2 concentration as a function of time can be seen for different caprock porosities (Fig. 11.a). The results indicated that the case with lower porosity offers a smaller pore volume for H_2 diffusion. Consequently, the concentration profile defined as the ratio of H_2 concentration to available pore volume, is the same in all cases. However, the loss is different and proportional to ϕ as can be seen in Fig. 11.b and Table 2. This is also consistent with the semi-analytical solution, where the H_2 loss is directly proportional to ϕ. Thus, a less porous caprock might be a more suitable option for UHS, as it offers much less space for H_2 diffusion.

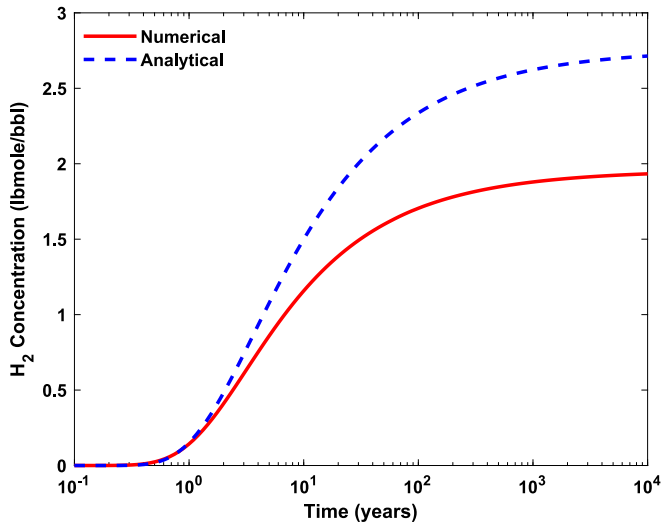

Fig. 7. H_2 concentration profiles at 5 ft. above the caprock-reservoir interface and at 4000 psi obtained from the numerical simulation and the analytical solution.

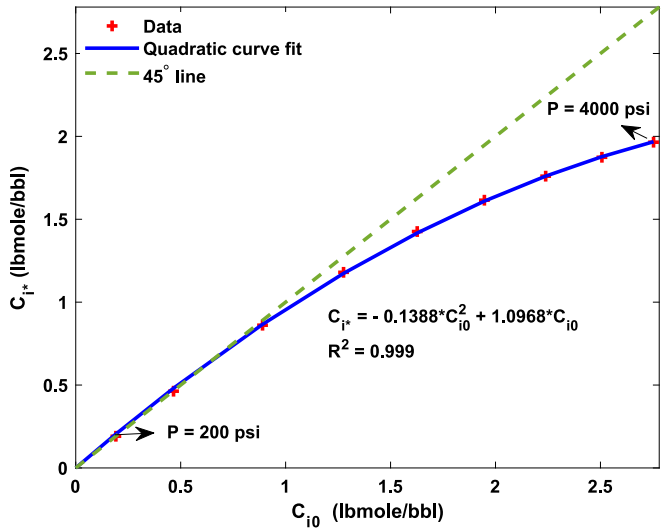

Fig. 8. Relation between C_{i^*} and C_{i0} for the pressure range of 200–4000 psi.

4.3.2. Diffusion coefficient

The amount of H_2 loss due to the diffusion process into the caprock depends mainly on the assigned D_i^a. In this study, different values (10^{-7} to 10^{-11} m^2/s) reported in the literature for H_2 diffusion through the caprock were used for D_i^a [34–38,60]. The results obtained are shown in Fig. 12. The simulations were performed at a pressure of 3000 psi where Z_{C1} was 5 %.

It was found that the H_2 concentration in the caprock increases sharply in the model with the D_i^a value of 10^{-7} m^2/s, indicating a rapid diffusion process. In this case, the H_2 concentration in the gas phase reaches the maximum value of 1.78 lbmole/bbl in less than 200 years. However, the build-up of H_2 concentration in the caprock at a D_i^a value of 10^{-11} m^2/s is very slow (Fig. 12.a). Table 3 gives the values of the different parameters used to assess H_2 diffusion in the caprock. As this table shows, the loss is proportional to the square root of D_i^a. These results underline the importance of D_i^a for a correct estimation of H_2 losses for a safe and efficient UHS.

4.3.3. Reservoir pressure

A candidate depleted gas reservoir could be under different pressures once chosen for H_2 storage [22]. Thus, H_2 storage was simulated in different models for a pressure of 500 to 4000 psi and a temperature of 92 to 205 °F. In these models, Z_{C1} was 5 %. It should be noted that the diffusion coefficient can also be a function of pressure. However, to better understand the impacts of pressure on H_2 diffusion, a constant D_i^a value was assumed for all cases. The H_2 concentration in the gas phase of the caprock at different pressures is shown in Fig. 13.a. At a pressure of 4000 psi, the final H_2 concentration (C_{i^*}) in the gas phase is 2.05 lbmole/bbl, while at a pressure of 500 psi, this value becomes 0.46 lbmole/bbl.

At higher pressure, a higher H_2 concentration in the reservoir is possible, i.e., a higher C_{i0}, and this can lead to a higher H_2 concentration in the caprock. However, it should be noted that a comparatively lower C_{i^*} can be expected at higher pressure, as shown in Fig. 8. Moreover, for the same initial Z_{C1}, there is lower gas saturation at higher pressure, which in turn limits H_2 diffusion. Fig. 13.b shows that n_i/A increases as the pressure increases from 500 to 3000 psi, but the loss is almost the same at 3000 and 4000 psi. Thus, while the total loss of H_2 loss may be greater at higher pressure, the final fractional loss of injected H_2 is less.

Table 4 provides the parameters of the concentration profiles at different pressures. It seems that by increasing the pressure, the gas saturation decreases (resulting in a lower loss) and C_{i^*} increases (resulting in a higher loss). The simultaneous effect of these two parameters at different pressures can be seen in this table. It is noteworthy that at pressures of 4000 and 3000 psi, the increase in C_{i^*} is almost proportional to the decrease in gas saturation. Thus, almost the same parameters were resulted at these pressures.

4.4. Comparing numerical and semi-analytical solutions

In this section, the performance of the presented semi-analytical solution for estimating H_2 loss into the caprock is investigated. For this purpose, 1-D models with different properties were built. The thermodynamic relations in Figs. 8 and 9 can be used to evaluate n_i. For example, if the relationship between the term $\frac{\partial(\ln f_i)}{\partial(\ln y_i)}$ vs. $\frac{C_i}{C_{i^*}}$ at a pressure of 3000 psi (Fig. 9) was used, n_i can be expressed as follows:

$$n_i \Big/ A = 1.275 \phi S_g C_{i^*} \sqrt{D_i} \sqrt{t}, \tag{27}$$

Fig. 14 shows the comparison of H_2 loss as a function of time between the proposed semi-analytical solution and the numerical simulation. The results were compared over a relevant time period of 100 years, where the systems were semi-infinite. It can be seen that n_i/A shows a linear trend with the square root of time. As Fig. 14 suggests, the trends of n_i/A predicted by the semi-analytical approach agree very well with those of the numerical simulation. The case with the highest porosity (5 %) and pressure (3000 psi) has the highest loss per unit area and the case with the lowest value of D_i^a (10^{-10} m^2/s) and porosity (2.5 %) has the slowest loss per unit area. It seems that the proposed semi-analytical solution can be efficiently used to predict the H_2 loss in the semi-infinite state.

5. Three-dimensional simulation study

In this section, an attempt was made to evaluate the H_2 diffusion in a cyclic H_2 storage operation using three-dimensional (3-D) models. In contrast to the 1-D models, these 3-D models have 30 blocks in the X and Y directions. Reservoir permeability in X, Y, and Z directions were 20, 20, and 2 md, respectively. Two different 3-D cases were considered. The first 3-D model represents a situation with strong H_2 diffusion, where ϕ was 10 % and D_i^a was 10^{-8} m^2/s. The second case shows a situation with less intense diffusion. In this case, ϕ and D_i^a were 5 % and 10^{-9} m^2/s, respectively and in both models Z_{C1} in the caprock was 5 %.

The model was initialized with C_1 as the existing gas in the reservoir and the initial reservoir pressure and temperature were 3000 psi and 173 °F, respectively. The injection and production operations were performed through a well located at the center of the model and the well

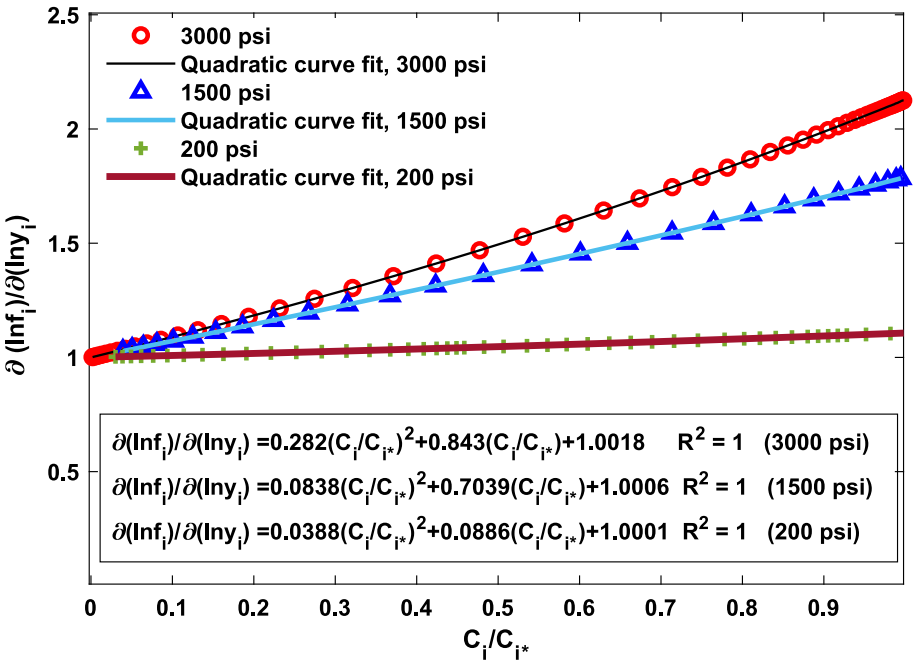

Fig. 9. Variation of the term $\frac{\partial(lnf_i)}{\partial(lny_i)}$ vs. $\frac{C_i}{C_{i^*}}$ at 200, 1500, and 3000 psi pressures.

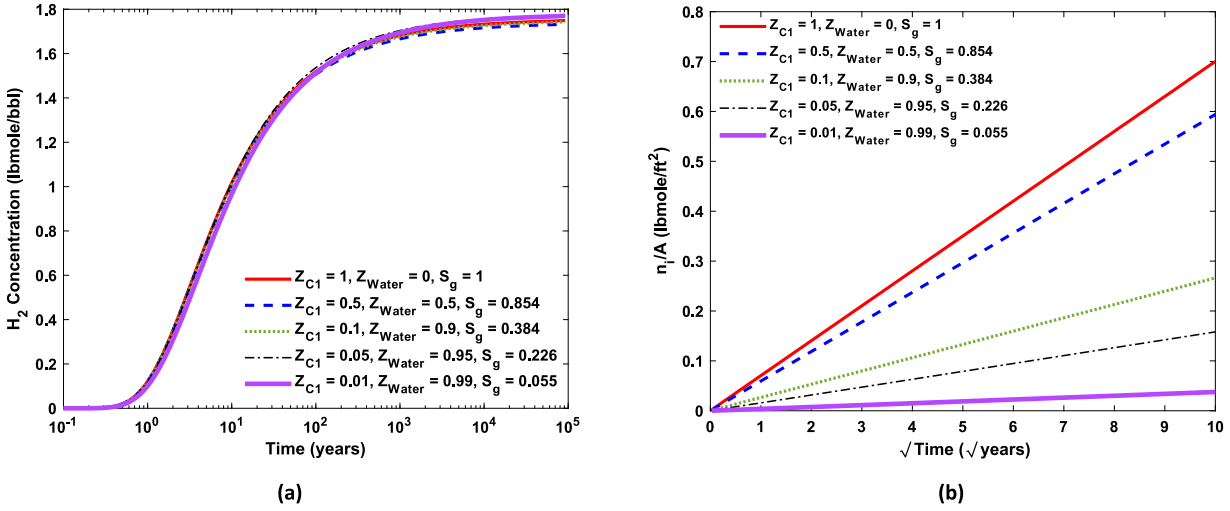

Fig. 10. Verifying the effect of caprock gas saturation: (a) H_2 concentration profiles in the gas phase of the caprock at 5 ft. above the caprock-reservoir interface and (b) Cumulative loss in the caprock versus square root of time after 100 years.

Table 1
Parameters of H_2 concentration profile in the caprock for different gas saturations.

Parameter	Unit	S_g				
		1	0.854	0.384	0.226	0.055
$n_{i,30}$	lbmole	153.51	130.05	58.27	34.59	8.23
$\overline{J_{i,30}}\phi S_g$	$\frac{lbmole}{ft^2 year}$	0.01279	0.01084	0.00486	0.00288	0.00069
$A_0\phi S_g$	$\frac{lbmole}{ft^2\sqrt{year}}$	0.06949	0.05463	0.02448	0.01451	0.00345

was completed at the top of the reservoir. Production with 50 Mscf/day was performed in the first 3 years followed by 1 year of H_2 injection with a rate of 25 Mscf/day. The injected H_2 at this stage could act as cushion gas. Then a 30-year cyclic H_2 injection was performed. In each cycle, H_2 was injected at a rate of 25 Mscf/day for 6 months. This was followed by a production rate of 37.5 Mscf/day for 4 months, 2 months after the injection. Fig. 15 shows a cross-section of the H_2 mole fraction distribution in the gas phase of the reservoir and the caprock for Case 1. Fig. 16 shows the net cumulative amount of H_2 injection together with H_2 diffusion into the caprock for Case 1 and Case 2. This figure also

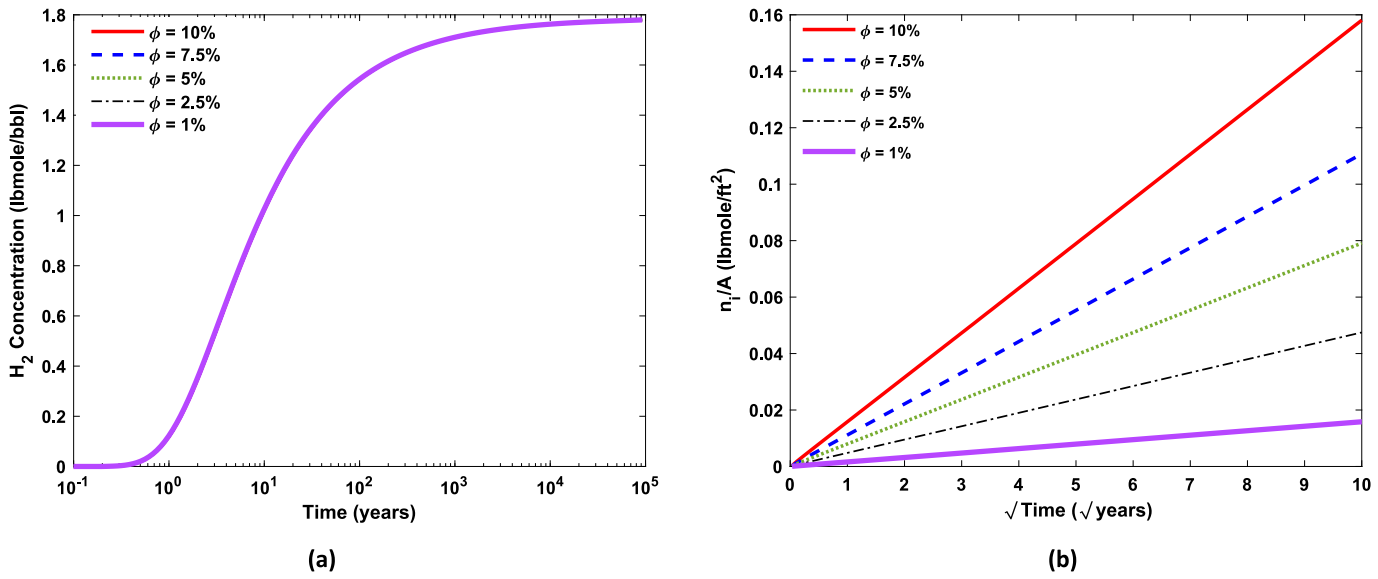

Fig. 11. Verifying the effect of caprock porosity: (a) H_2 concentration profiles in the gas phase of caprock at 5 ft. above the caprock-reservoir interface and (b) Cumulative loss in the caprock versus square root of time after 100 years.

Table 2
Parameters of H_2 concentration profile in the caprock for different caprock porosity.

Parameter	Unit	ϕ (%)				
		10	7.5	5	2.5	1
$n_{i,30}$	lbmole	34.59	24.24	17.32	10.40	3.47
$\overline{J_{i,30}}\phi S_g$	$\frac{lbmole}{ft^2 year}$	0.00288	0.00202	0.00144	0.00087	0.00029
$A_0\phi S_g$	$\frac{lbmole}{ft^2\sqrt{year}}$	0.01451	0.01037	0.00752	0.00459	0.00156

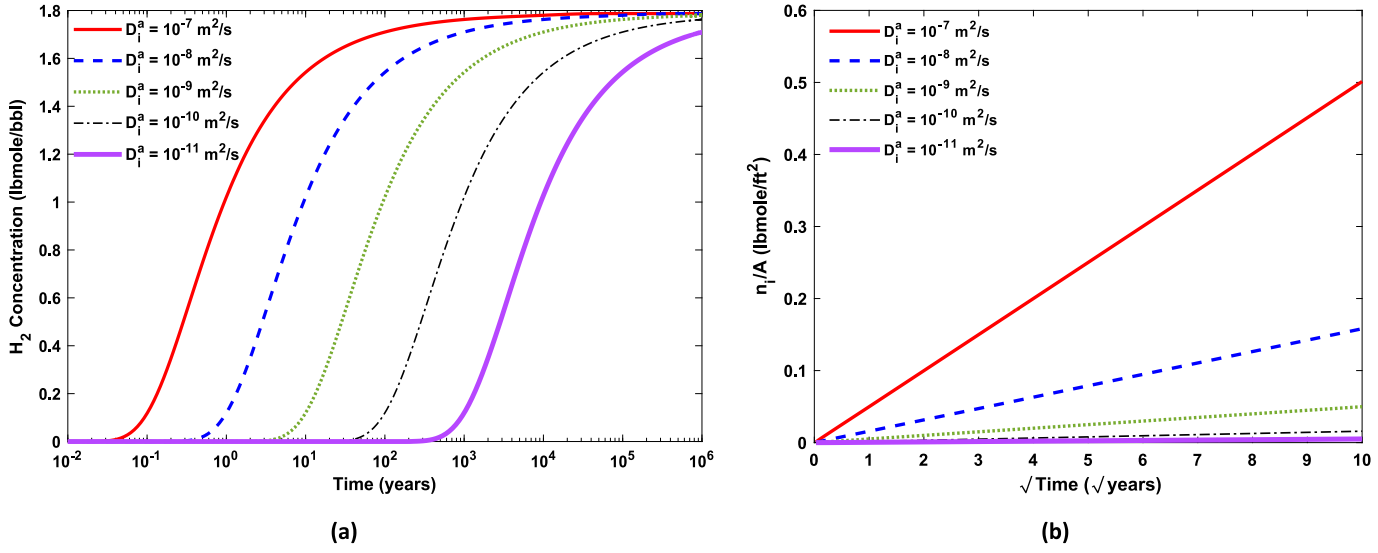

Fig. 12. Verifying the effect of D_i^a: (a) H_2 concentration profiles in the gas phase of caprock at 5 ft above the caprock-reservoir interface and (b) Cumulative loss in the caprock versus square root of time after 100 years.

shows the cumulative H_2 losses calculated with the semi-analytical solution. At the beginning of the cyclic H_2 injection, the average reservoir pressure was 2250 psi. Since A and C_{i0} fluctuated during the 30 years of cyclic injection, average values for A and C_{i0} over the 30 years were used in the semi-analytical solution for both cases. It should be noted that the differences between the approaches specifically for Case 1 are due to the use of the average values of A and C_{i0} over the 30 years.

Considerable diffusion was observed in Case 1 with an H_2 loss of 5.5 % during the 30-years of cyclic operation, while the H_2 loss in the second case was 1.16 %. With even less favorable conditions for H_2 diffusion (ϕ is 1 % and D_i^a is 10^{-9} m^2/s), the H_2 loss was 0.223 % during the 30 years of cyclic UHS operation. As also suggested by the semi-analytical

Table 3
Parameters of H_2 concentration profile in the caprock for different D_i^a.

Parameter	Unit	D_i^a (m^2/s)				
		10^{-7}	10^{-8}	10^{-9}	10^{-10}	10^{-11}
$n_{i,30}$	lbmole	109.65	34.59	10.95	3.49	1.11
$\overline{J_{i,30}}\phi S_g$	$\frac{lbmole}{ft^2 year}$	0.00914	0.00288	0.00091	0.00029	0.00009
$A_0\phi S_g$	$\frac{lbmole}{ft^2\sqrt{year}}$	0.04654	0.01451	0.00436	0.00122	0.00032

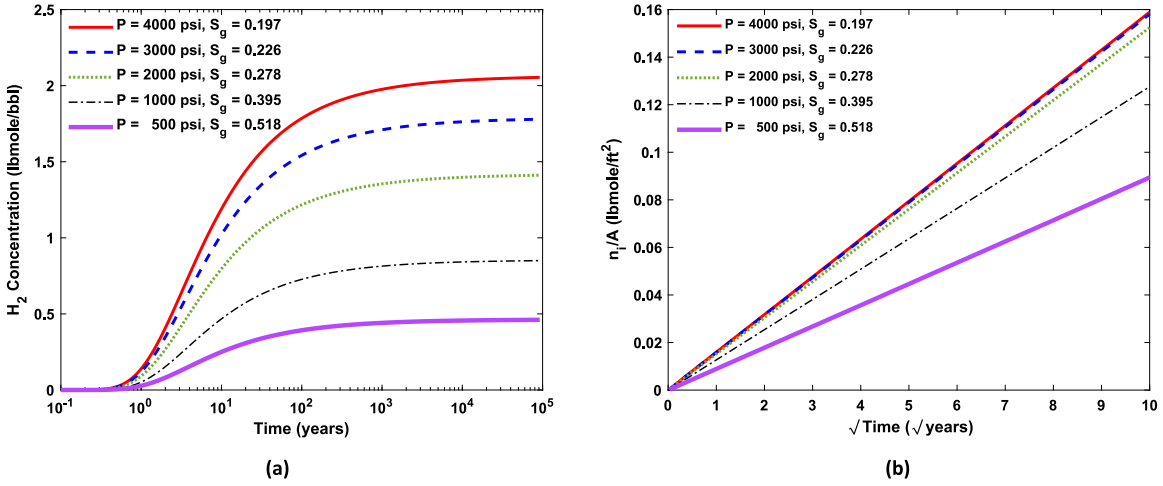

Fig. 13. Verifying the effect of pressure: (a) H_2 concentration profiles in the gas phase of caprock at 5 ft. above the caprock-reservoir interface and (b) Cumulative loss in the caprock versus square root of time after 100 years.

Table 4
Parameters of H_2 concentration profile in the caprock for different pressures

Parameter	Unit	P (psi)				
		4000	3000	2000	1000	500
$n_{i,30}$	lbmole	34.79	34.59	33.34	27.89	19.57
$\overline{J_{i,30}}\phi S_g$	$\frac{lbmole}{ft^2 year}$	0.00290	0.00288	0.00278	0.00232	0.00163
$A_0\phi S_g$	$\frac{lbmole}{ft^2\sqrt{year}}$	0.01491	0.01451	0.01382	0.01141	0.00797

solution, these results indicate that for the same value of D_i^a and the same reservoir conditions, the H_2 flux into the caprock is proportional to ϕ.

It should be noted that the H_2 diffusion rate is higher in the initial phase of operation, but the loss is expected to decrease with time. Fig. 15 also illustrates that H_2 below the caprock is concentrated near the injection/withdrawal well during the cyclic storage operation. The cumulative H_2 losses into the caprock determined by the numerical simulation for Case 1 and Case 2 were 2.098×10^4 and 4.417×10^3 lbmole, respectively. In addition, the cumulative H_2 losses obtained from the semi-analytical solution for Case 1 and Case 2 were 1.963×10^4 lbmole and 3.991×10^3 lbmole, respectively. Based on these results and the cumulative loss profiles (shown in Fig. 16), a fairly good agreement between the numerical and the semi-analytical approach can be seen.

6. Discussion

In this work, H_2 diffusion into the caprock was analyzed by considering overlying formations as a semi-infinite system. Representative analytical, semi-analytical, and numerical solutions based on the initial and boundary conditions were used to study the H_2 diffusion into the caprock in depleted gas reservoirs. The proposed semi-analytical solution and the loss fraction criterion can be used for proper estimation of the extent of H_2 loss due to diffusion during UHS in depleted gas reservoirs.

At high reservoir pressure, the concentration profiles of the diffused H_2 due to the chemical potential are different from those of the concentration gradient. In fact, the chemical potential gradient results in a lower final concentration in the caprock, i.e., C_{i^*}. With a suitable equation of state, one can relate the H_2 concentration in the reservoir and directly below the caprock (C_{i0}) to C_{i^*}. In summary, one may overestimate the H_2 diffusion if the concentration gradient is used at elevated reservoir pressure to predict H_2 diffusion into the caprock.

As Fig. 8 suggests, the boundary concentrations at the reservoir (C_{i0}) and caprock (C_{i^*}) are the same at very low reservoir pressures. However, at high reservoir pressures, lower values for C_{i^*} are expected compared to C_{i0}. This fact leads to a relatively lower final fractional loss of H_2 at elevated reservoir pressures.

Long-term contact of hydrocarbon gas with the caprock provides the opportunity for diffusion of hydrocarbon gas into the caprock. The diffusion of hydrocarbon gas into the caprock would create more space for H_2 diffusion in the caprock by reducing water saturation [55–57]. It should be noted that impacts of the previously diffused hydrocarbon gas must be considered otherwise H_2 diffusion into the caprock will be underestimated. It is beneficial to study the factors that control the

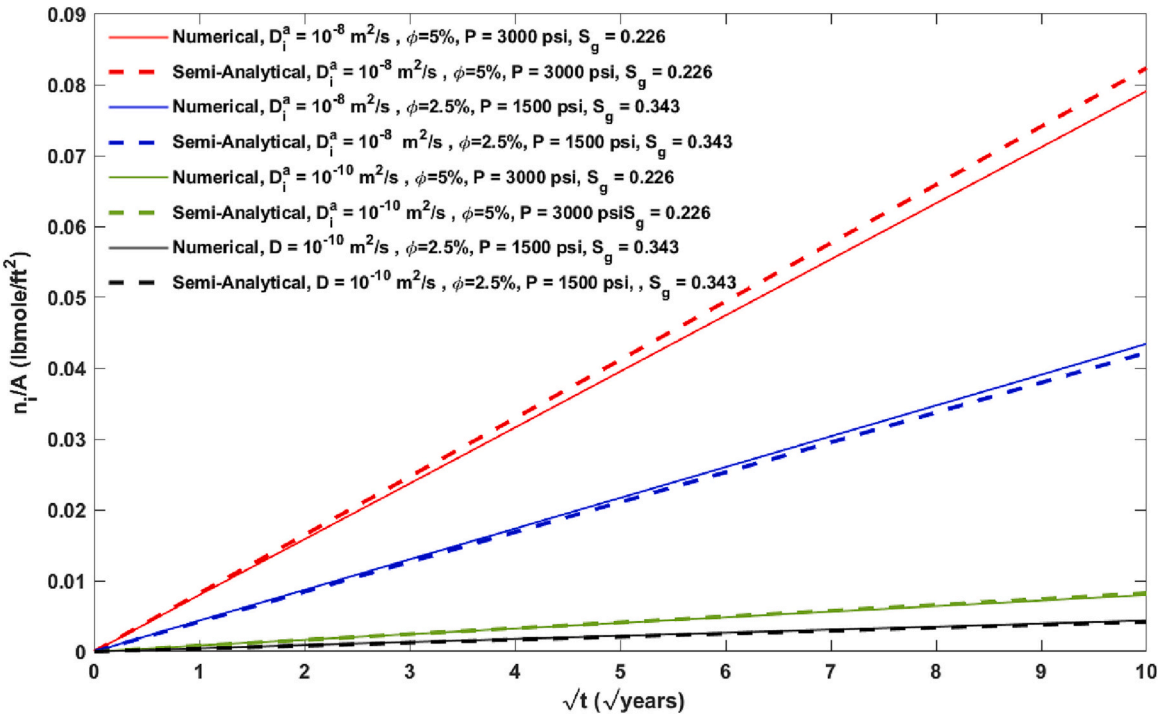

Fig. 14. Comparison of H_2 loss as a function of time between the proposed semi-analytical solution and the numerical simulation.

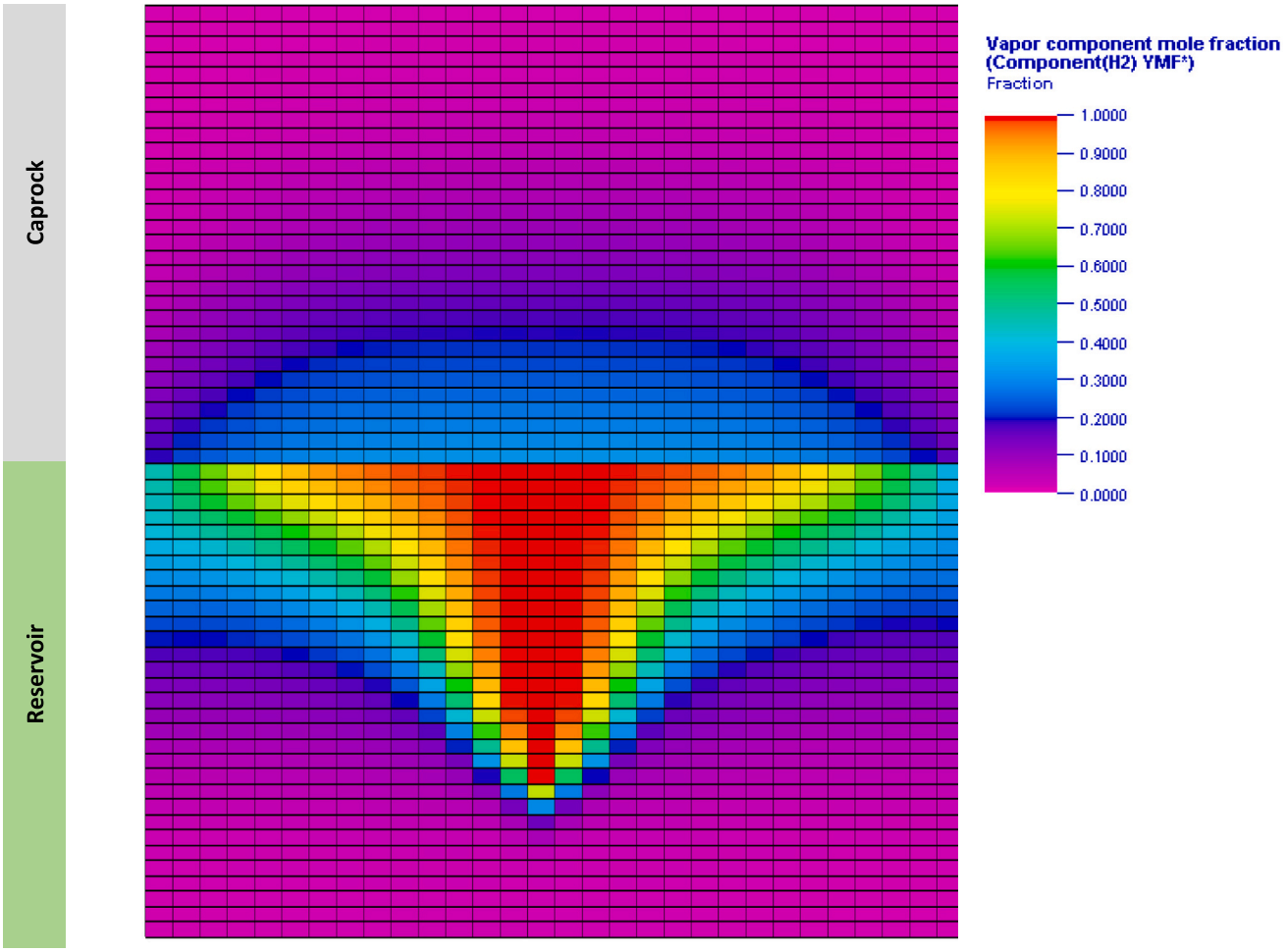

Fig. 15. H_2 component mole fraction distribution in the gas phase of reservoir and caprock for 3-D model in the first case.

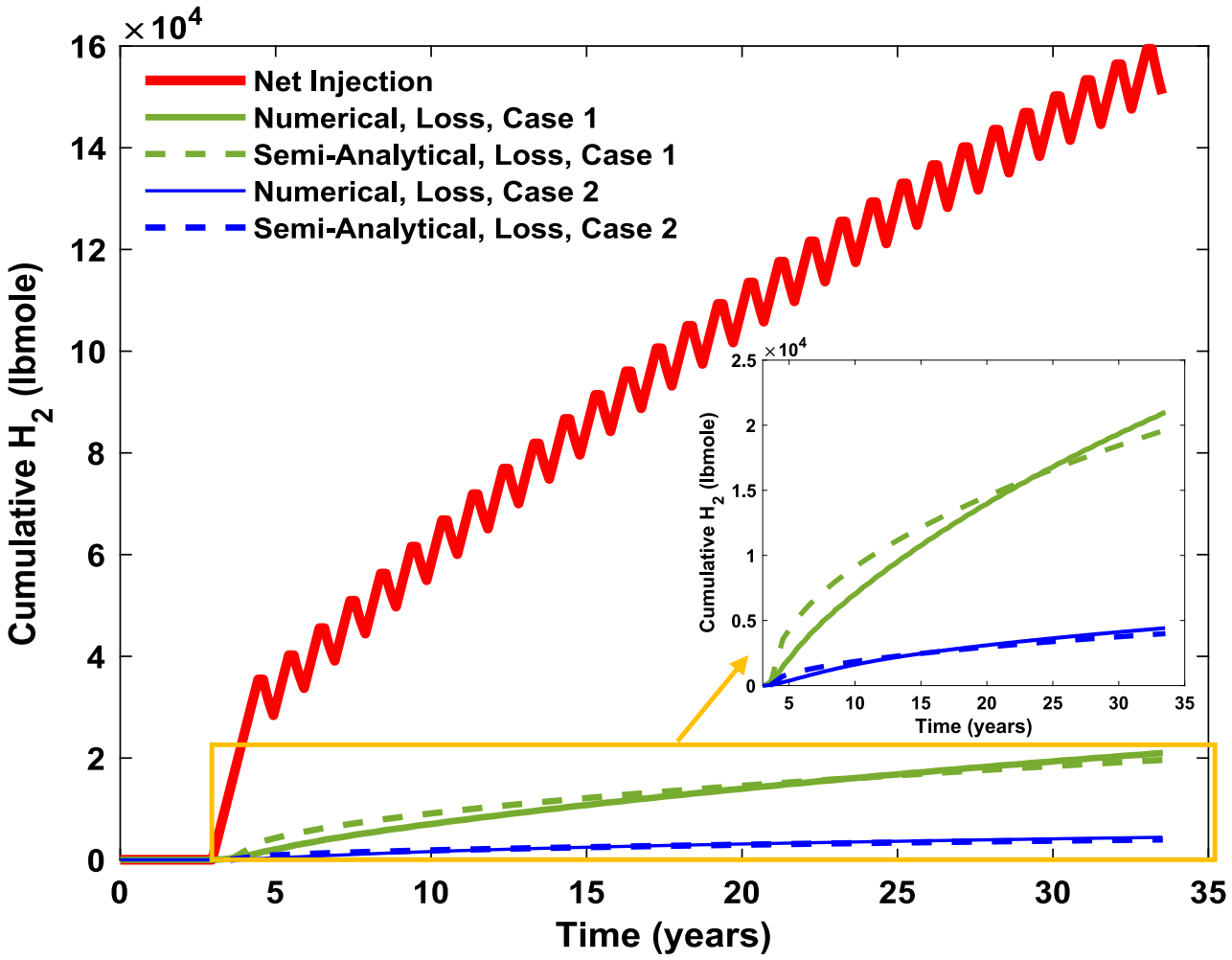

Fig. 16. The net amount of injected H_2 and the amount diffused into the caprock for both cases using numerical and semi-analytical solutions.

diffusion of hydrocarbon gas into the caprock, such as gas-caprock interactions, caprock microfractures, gas-water thermodynamic conditions, and heterogeneities [55,58].

The results showed that even the presence of a small total mole fraction of C_1 in the caprock would lead to considerable gas saturation. For example, at a pressure of 3000 psi and a temperature of 173 °F, a gas saturation of 5.5 % was obtained for a fraction of 0.01 Z_{C1}. Only a very small amount of water also appears in the gas phase due to the thermodynamic conditions between water and C_1. Thus, the gas phase has a lower density than the liquid phase which consists mainly of water. As a result, the gas phase occupies a large volume, which consequently results in high gas saturation in the caprock.

It should be noted that in this work, C_1 was assumed to be the pre-diffused hydrocarbon gas into the caprock. Thermodynamic conditions in the caprock may be different when other hydrocarbon gases are present. Further studies on the possible impacts of other hydrocarbon gases on H_2 diffusion are recommended.

The probable interactions of H_2 with brine and caprock were not the focus of this study. These interactions may change caprock properties and influence the diffusion process of H_2. The role of the caprock heterogeneity can also be considered in future studies.

Based on the semi-analytical solution, it can be said that the H_2 loss is directly proportional to ϕ, A, C_{i*} and the square root of D_i^a. Moreover, similar to the spontaneous imbibition process, the H_2 loss shows a linear trend against the square root of time during the semi-infinite period. Moreover, the semi-analytical solution can be used to evaluate H_2 diffusion during a cyclic UHS in three-dimensional models if proper estimates of the average A and C_{i0} are used.

In the 3-D models, Case 1 (with 10 % of ϕ and 10^{-8} m^2/s of D_i^a) showed higher H_2 loss compared to Case 2 (with 5 % of ϕ and 10^{-9} m^2/s of D_i^a). The amount of H_2 loss in Cases 1 and 2 were 5.5 and 1.16 % during the 30-years of cyclic operation, respectively. The results highlight the importance of proper caprock characterization for more precise estimation of H_2 loss in UHS.

7. Conclusions

The present study examined the process of molecular diffusion loss of hydrogen into caprock during hydrogen storage in depleted gas reservoirs. The chemical potential gradient was used as the driving mechanism of hydrogen diffusion in the complex multi-component hydrocarbon-water-hydrogen system. The effect of previously diffused hydrocarbon gas in the caprock was also considered.

- Exploiting the similarities between the partial differential equation describing nonlinear diffusion and spontaneous imbibition systems, we have presented a semi-analytical solution for the system that holds for one-dimensional and semi-infinite conditions. Based on the semi-analytical solution, we were able to accurately calculate the total loss of hydrogen as a function of time and the fraction of hydrogen lost compared to the hydrogen stored in the reservoir. We also reproduced hydrogen diffusion in one- and three-dimensional models using numerical simulations.

- The semi-analytical solution suggests that hydrogen loss due to diffusion is directly proportional to the area between the caprock and the reservoir exposed to hydrogen, the porosity of the caprock, the gas saturation of the caprock, the equilibrium hydrogen concentration in the caprock based on chemical potential, the square root of the diffusion coefficient, and the square root of time.
- Using the semi-analytical method, good agreements were obtained for the hydrogen loss with the numerical simulation approach. It was also shown that the hydrogen loss during the relevant time when the system is in the semi-infinite state has a linear trend over the square root of time.
- The simulation results showed lower boundary concentration in the caprock compared to that of the reservoir when the chemical potential gradient was used as the driving mechanism for diffusion. This effect was significant at the high pressures relevant for hydrogen storage.
- The results revealed that the presence of pre-diffused hydrocarbon gas in the caprock enhances hydrogen diffusion into the caprock by providing more space in the gas phase for hydrogen diffusion.
- At low pressure, the influence of the chemical potential decreases and an analytical solution with a constant diffusion coefficient and the same boundary concentration as in the reservoir was derived. Very good agreement was obtained between the numerical and analytical solutions at low pressure, where a similar mass flux was expected due to chemical and concentration gradients.
- Higher reservoir pressure is expected to result in higher hydrogen loss, as the hydrogen concentration is higher at higher reservoir pressure and the hydrogen diffusion flux is enhanced. However, at higher pressures, relatively lower final concentrations of hydrogen were expected in the caprock compared to the reservoir, which may result in a lower final fractional loss.

The results obtained and presented in this study can provide a deeper insight into the mechanisms and influencing parameters of hydrogen diffusion through the caprock. They can also be useful for the selection of suitable sites for underground hydrogen storage. Further studies are needed to assess the impact of caprock heterogeneity and to investigate the effects of possible geochemical and biochemical reactions on hydrogen diffusion through the caprock.

CRediT authorship contribution statement

Mojtaba Ghaedi: Writing – original draft, Software, Methodology, Validation, Formal analysis. **Pål Østebø Andersen:** Supervision, Writing – review & editing, Methodology, Formal analysis. **Raoof Gholami:** Supervision, Writing – review & editing, Methodology, Formal analysis.

Declaration of competing interest

The authors declare that they have no known competing financial interests or personal relationships that could have appeared to influence the work reported in this paper.

Data availability

Data will be made available on request.

References

[1] N. Heinemann, M.G. Booth, R.S. Haszeldine, M. Wilkinson, J. Scafidi, K. Edlmann, Hydrogen storage in porous geological formations – onshore play opportunities in the midland valley (Scotland, UK), Int. J. Hydrog. Energy 43 (2018) 20861–20874, https://doi.org/10.1016/j.ijhydene.2018.09.149.

[2] A. Hassanpouryouzband, K. Adie, T. Cowen, E.M. Thaysen, N. Heinemann, I. B. Butler, M. Wilkinson, K. Edlmann, Geological hydrogen storage: geochemical reactivity of hydrogen with sandstone reservoirs, ACS Energy Lett. (2022) 2203–2210, https://doi.org/10.1021/acsenergylett.2c01024.

[3] A. Hassanpouryouzband, E. Joonaki, K. Edlmann, R.S. Haszeldine, Offshore geological storage of hydrogen: is this our best option to achieve net-Zero? ACS Energy Lett. 6 (2021) 2181–2186, https://doi.org/10.1021/acsenergylett.1c00845.

[4] S. Flesch, D. Pudlo, D. Albrecht, A. Jacob, F. Enzmann, Hydrogen underground storage—petrographic and petrophysical variations in reservoir sandstones from laboratory experiments under simulated reservoir conditions, Int. J. Hydrog. Energy 43 (2018) 20822–20835, https://doi.org/10.1016/j.ijhydene.2018.09.112.

[5] N.S. Muhammed, B. Haq, D. al Shehri, A. Al-Ahmed, M.M. Rahman, E. Zaman, A review on underground hydrogen storage: Insight into geological sites, influencing factors and future outlook, Energy Reports 8 (2022) 461–499, https://doi.org/10.1016/j.egyr.2021.12.002.

[6] J. Juez-Larré, S. van Gessel, R. Dalman, G. Remmelts, R. Groenenberg, Assessment of underground energy storage potential to support the energy transition in the Netherlands, First Break 37 (2019) 57–66, https://doi.org/10.3997/1365-2397.n0039.

[7] T. Wang, L. Ao, B. Wang, S. Ding, K. Wang, F. Yao, J.J.K. Daemen, Tightness of an underground energy storage salt cavern with adverse geological conditions, Energy 238 (2022), 121906, https://doi.org/10.1016/j.energy.2021.121906.

[8] K. Zhao, Y. Liu, Y. Li, H. Ma, W. Hou, C. Yu, H. Liu, C. Feng, C. Yang, Feasibility analysis of salt cavern gas storage in extremely deep formation: a case study in China, J. Energy Storage 47 (2022), 103649, https://doi.org/10.1016/j.est.2021.103649.

[9] P.G. Haddad, M. Ranchou-peyruse, M. Guignard, J. Mura, F. Casteran, Environmental Science Geological Storage of Hydrogen in Deep Aquifers – An Experimental Multidisciplinary Study, 2022, https://doi.org/10.1039/d2ee00765g.

[10] T. Bai, P. Tahmasebi, Coupled hydro-mechanical analysis of seasonal underground hydrogen storage in a saline aquifer, J. Energy Storage 50 (2022), 104308, https://doi.org/10.1016/j.est.2022.104308.

[11] A. Amid, D. Mignard, M. Wilkinson, Seasonal storage of hydrogen in a depleted natural gas reservoir, Int. J. Hydrog. Energy 41 (2016) 5549–5558, https://doi.org/10.1016/j.ijhydene.2016.02.036.

[12] C. Hemme, W. van Berk, Hydrogeochemical modeling to identify potential risks of underground hydrogen storage in depleted gas fields, Appl. Sci. (Switzerland) 8 (2018) 1–19, https://doi.org/10.3390/app8112282.

[13] D.G. Caglayan, N. Weber, H.U. Heinrichs, J. Linßen, M. Robinius, P.A. Kukla, D. Stolten, Technical potential of salt caverns for hydrogen storage in Europe, Int. J. Hydrog. Energy 45 (2020) 6793–6805, https://doi.org/10.1016/j.ijhydene.2019.12.161.

[14] Y. Zheng, Q. Wanyan, X. Qiu, Y. Kou, L. Ran, X. Lai, S. Wu, New technologies for site selection and evaluation of salt-cavern underground gas storages, Nat. Gas Ind. B 7 (2020) 40–48, https://doi.org/10.1016/j.ngib.2019.06.002.

[15] L. Lankof, R. Tarkowski, Assessment of the potential for underground hydrogen storage in bedded salt formation, Int. J. Hydrog. Energy 45 (2020) 19479–19492, https://doi.org/10.1016/j.ijhydene.2020.05.024.

[16] J.D.O. Williams, J.P. Williamson, D. Parkes, D.J. Evans, K.L. Kirk, N. Sunny, E. Hough, H. Vosper, M.C. Akhurst, Does the United Kingdom have sufficient geological storage capacity to support a hydrogen economy? Estimating the salt cavern storage potential of bedded halite formations, J. Energy Storage 53 (2022) 105109, https://doi.org/10.1016/j.est.2022.105109.

[17] K. Luboń, R. Tarkowski, Numerical simulation of hydrogen injection and withdrawal to and from a deep aquifer in NW Poland, Int. J. Hydrog. Energy 45 (2020) 2068–2083, https://doi.org/10.1016/J.IJHYDENE.2019.11.055.

[18] A. Sainz-Garcia, E. Abarca, V. Rubi, F. Grandia, Assessment of feasible strategies for seasonal underground hydrogen storage in a saline aquifer, Int. J. Hydrog. Energy 42 (2017) 16657–16666, https://doi.org/10.1016/J.IJHYDENE.2017.05.076.

[19] N. Heinemann, J. Scafidi, G. Pickup, E.M. Thaysen, A. Hassanpouryouzband, M. Wilkinson, A.K. Satterley, M.G. Booth, K. Edlmann, R.S. Haszeldine, Hydrogen storage in saline aquifers: the role of cushion gas for injection and production, Int. J. Hydrog. Energy 46 (2021) 39284–39296, https://doi.org/10.1016/j.ijhydene.2021.09.174.

[20] M. Lysyy, M. Fernø, G. Ersland, Seasonal hydrogen storage in a depleted oil and gas field, Int. J. Hydrog. Energy 46 (2021) 25160–25174, https://doi.org/10.1016/j.ijhydene.2021.05.030.

[21] M. Zamehrian, B. Sedaee, Underground hydrogen storage in a partially depleted gas condensate reservoir: influence of cushion gas, J. Pet. Sci. Eng. 212 (2022), 110304, https://doi.org/10.1016/j.petrol.2022.110304.

[22] D. Zivar, S. Kumar, J. Foroozesh, Underground hydrogen storage: a comprehensive review, Int. J. Hydrog. Energy 46 (2021) 23436–23462, https://doi.org/10.1016/j.ijhydene.2020.08.138.

[23] T.M.R.B. Visser, Seasonal Hydrogen Storage in Depleted Gas Reservoirs: A Feasibility Study for The Netherlands, Delft University of Technology, 2020.

[24] M. Hosseini, J. Fahimpour, M. Ali, A. Keshavarz, S. Iglauer, Capillary Sealing Efficiency Analysis of Caprocks: Implication for Hydrogen Geological Storage, 2022, https://doi.org/10.1021/acs.energyfuels.2c00281.

[25] M. Hosseini, M. Ali, J. Fahimpour, A. Keshavarz, S. Iglauer, Assessment of rock-hydrogen and rock-water interfacial tension in shale, evaporite and basaltic rocks, J. Nat. Gas Sci. Eng. 106 (2022), 104743, https://doi.org/10.1016/J.JNGSE.2022.104743.

[26] D.W. Jayasekara, P.G. Ranjith, W.A.M. Wanniarachchi, T.D. Rathnaweera, Understanding the chemico-mineralogical changes of caprock sealing in deep saline CO2 sequestration environments: a review study, J. Supercrit. Fluids 161 (2020), 104819, https://doi.org/10.1016/J.SUPFLU.2020.104819.

[27] J.P. Bensing, D. Misch, L. Skerbisch, R.F. Sachsenhofer, Hydrogen-induced calcite dissolution in amaltheenton formation claystones: implications for underground hydrogen storage caprock integrity, Int. J. Hydrog. Energy 47 (2022) 30621–30626, https://doi.org/10.1016/J.IJHYDENE.2022.07.023.
[28] K. Labus, R. Tarkowski, Modeling hydrogen – rock – brine interactions for the jurassic reservoir and cap rocks from polish lowlands, Int. J. Hydrog. Energy 47 (2022) 10947–10962, https://doi.org/10.1016/J.IJHYDENE.2022.01.134.
[29] D. Wolff-Boenisch, H.R. Abid, J.E. Tucek, A. Keshavarz, S. Iglauer, Importance of clay-H2 interactions for large-scale underground hydrogen storage, Int. J. Hydrog. Energy (2023), https://doi.org/10.1016/J.IJHYDENE.2022.12.324.
[30] Z. Bo, L. Zeng, Y. Chen, Q. Xie, Geochemical reactions-induced hydrogen loss during underground hydrogen storage in sandstone reservoirs, Int. J. Hydrog. Energy 46 (2021) 19998–20009, https://doi.org/10.1016/J.IJHYDENE.2021.03.116.
[31] R. Gholami, Hydrogen storage in geological porous media: solubility, mineral trapping, H2S generation and salt precipitation, J. Energy Storage 59 (2023), 106576, https://doi.org/10.1016/J.EST.2022.106576.
[32] M.S.A. Perera, A review of underground hydrogen storage in depleted gas reservoirs: insights into various rock-fluid interaction mechanisms and their impact on the process integrity, Fuel 334 (2023), 126677, https://doi.org/10.1016/J.FUEL.2022.126677.
[33] R. Tarkowski, B. Uliasz-Misiak, Towards underground hydrogen storage: a review of barriers, Renew. Sust. Energ. Rev. 162 (2022), 112451, https://doi.org/10.1016/j.rser.2022.112451.
[34] A. Keshavarz, H. Abid, M. Ali, S. Iglauer, Hydrogen diffusion in coal: implications for hydrogen geo-storage, J. Colloid Interface Sci. 608 (2022) 1457–1462, https://doi.org/10.1016/j.jcis.2021.10.050.
[35] J. Liu, S. Wang, F. Javadpour, Q. Feng, L. Cha, Hydrogen Diffusion in Clay Slit : Implications for the Geological Storage, 2022, https://doi.org/10.1021/acs.energyfuels.2c01189.
[36] R.B. Gupta, A. Basile, T.N. Veziroğlu, Underground and pipeline hydrogen storage, in: Compendium of Hydrogen Energy: Volume 2: Hydrogen Storage, Distribution and Infrastructure, Elsevier, Cambridge, UK; Waltham, MA, USA; Kidlington, UK, 2016, https://doi.org/10.1016/C2014-0-02673-1.
[37] S.H. Bhimineni, T. Zhou, S. Mahmoodpour, M. Singh, W. Li, S. Bag, I. Sass, F. Müller-Plathe, Machine-Learning-Assisted Investigation of the Diffusion of Hydrogen in Brine by Performing Molecular Dynamics Simulation, 2022. http://arxiv.org/abs/2207.02966.
[38] M. Ghasemi, S. Omrani, S. Mahmoodpour, T. Zhou, Molecular dynamics simulation of hydrogen diffusion in water-saturated clay minerals; implications for underground hydrogen storage (UHS), Int. J. Hydrog. Energy 47 (2022) 24871–24885, https://doi.org/10.1016/j.ijhydene.2022.05.246.
[39] J. Crank, The Mathematics of Diffusion, Clarendon Press, 1975, https://doi.org/10.1021/ja01562a072.
[40] M. Gamal Rezk, J. Foroozesh, Uncertainty effect of CO2 molecular diffusion on oil recovery and gas storage in underground formations, Fuel 324 (2022), 124770, https://doi.org/10.1016/j.fuel.2022.124770.
[41] B.E. Poling, J.M. Prausnitz, John P. O'Connell, The Properties of Gases and Liquids, McGraw-Hill, 2001.
[42] GeoQuest, ECLIPSE Reference Manual, Schlumberger, 2022.
[43] B. Krooss, D. Leythaeuser, Molecular diffusion of light hydrocarbons in sedimentary rocks and its role in migration and dissipation of natural gas, AAPG Mem. 66 (1996) 173–185.
[44] D. Leythaeuser, R.G. Schaefer, A. Yükler, Diffusion of light hydrocarbons through near-surface rocks, Nature 284 (5756) (1980) 522–525, https://doi.org/10.1038/284522a0.
[45] D. Leythaeuser, R.G. Schaefer, A. Yukler, G. Bruch, F. Schlosser, K. Schmitt, B. Winden, Role of diffusion in primary migration of hydrocarbons, the american associaiion of petroleum geologists, Bulletin 66 (1982).
[46] D.B. McWhorter, D.K. Sunada, Exact integral solutions for two-phase flow, Water Resour. Res. 26 (1990) 399–413, https://doi.org/10.1029/WR026I003P00399.
[47] P.Ø. Andersen, A semi-analytical solution for shale gas production from compressible matrix including scaling of gas recovery, J. Nat. Gas Sci. Eng. 95 (2021), 104227, https://doi.org/10.1016/J.JNGSE.2021.104227.
[48] P.Ø. Andersen, Early- and late-time prediction of counter-current spontaneous imbibition, scaling analysis and estimation of the capillary diffusion coefficient, Transp. Porous Media (2023), https://doi.org/10.1007/s11242-023-01924-6.
[49] MATLAB, Natick, The MathWorks Inc., Massachusetts, 2022.
[50] D.Y. Peng, D.B. Robinson, A new two-constant equation of state, Ind. Eng. Chem. Fundam. 15 (1976) 59–64, https://doi.org/10.1021/i160057a011.
[51] S. Hogeweg, G. Strobel, B. Hagemann, Benchmark study for the simulation of underground hydrogen storage operations, Comput. Geosci. 2022 (2022) 1–12, https://doi.org/10.1007/S10596-022-10163-5.
[52] G. Wang, G. Pickup, K. Sorbie, E. Mackay, Numerical modelling of H2 storage with cushion gas of CO2 in subsurface porous media: filter effects of CO2 solubility, Int. J. Hydrog. Energy 47 (2022) 28956–28968, https://doi.org/10.1016/J.IJHYDENE.2022.06.201.
[53] G.Marselevna Shafikova, C.Hays Whitson, Analysis of Diffusion Models in Eclipse 300, 2013.
[54] I.D. Dumbrava, C.C. Cormos, Techno-economical evaluations of decarbonized hydrogen production based on direct biogas conversion using thermo-chemical looping cycles, Int. J. Hydrog. Energy 46 (2021) 23149–23163, https://doi.org/10.1016/j.ijhydene.2021.04.142.
[55] Y. Xue, J. Liu, X. Liang, X. Li, S. Wang, Z. Ma, S. Zhang, X. Jiao, Influence mechanism of brine-gas two-phase flow on sealing property of anisotropic caprock for hydrogen and carbon energy underground storage, Int. J. Hydrog. Energy (2022), https://doi.org/10.1016/J.IJHYDENE.2022.05.173.
[56] J.G. Wang, Y. Peng, Numerical modeling for the combined effects of two-phase flow, deformation, gas diffusion and CO2 sorption on caprock sealing efficiency, J. Geochem. Explor. 144 (2014) 154–167, https://doi.org/10.1016/J.GEXPLO.2013.12.011.
[57] Y. Xue, J. Liu, F. Dang, X. Liang, S. Wang, Z. Ma, Influence of CH4 adsorption diffusion and CH4-water two-phase flow on sealing efficiency of caprock in underground energy storage, Sustain. Energy Technol. Assess. 42 (2020), 100874, https://doi.org/10.1016/J.SETA.2020.100874.
[58] T. Bui, A. Phan, D.R. Cole, A. Striolo, Transport mechanism of guest methane in water-filled nanopores, J. Phys. Chem. C 121 (2017) 15675–15686, https://doi.org/10.1021/ACS.JPCC.7B02713/ASSET/IMAGES/LARGE/JP-2017-02713U_0010.JPEG.
[59] J. Goral, P. Panja, M. Deo, M. Andrew, S. Linden, J.O. Schwarz, A. Wiegmann, Confinement effect on porosity and permeability of shales, Scientific Reports 10 (1) (2020) 1–11, https://doi.org/10.1038/s41598-019-56885-y.
[60] E. Jacops, K. Wouters, G. Volckaert, H. Moors, N. Maes, C. Bruggeman, R. Swennen, R. Littke, Measuring the effective diffusion coefficient of dissolved hydrogen in saturated boom clay, Appl. Geochem. 61 (2015) 175–184, https://doi.org/10.1016/j.apgeochem.2015.05.022.